Off-equatorial orbits in strong gravitational fields near compact objectsII: halo motion around magnetic compact stars and magnetized black holes

J Kovář, O Kopáek, V Karas, Z Stuchlk

Off-equatorial orbits in strong gravitational fields near compact objects – II.

Halo motion around magnetic compact stars and magnetized black holes

J. Kovář[1,2], O. Kopáček[2], V. Karas[2] and Z. Stuchlík[1]

[1]Institute of Physics, Faculty of Philosophy and Science, Silesian University in Opava, Bezručovo nám. 13, CZ-746 01 Opava, Czech Republic
[2]Astronomical Institute, Academy of Sciences, Boční II, CZ-141 31 Prague, Czech Republic

E-mail: Jiri.Kovar@fpf.slu.cz

Abstract. Off-equatorial circular orbits with constant latitudes (halo orbits) of electrically charged particles exist near compact objects. In the previous paper, we discussed this kind of motion and demonstrated the existence of minima of the two-dimensional effective potential which correspond to the stable halo orbits.

Here, we relax previous assumptions of the pseudo-Newtonian approach for the gravitational field of the central body and study properties of the halo orbits in detail. Within the general relativistic approach, we carry out our calculations in two cases. Firstly, we examine the case of a rotating magnetic compact star. Assuming that the magnetic field axis and the rotation axis are aligned with each other, we study the orientation of motion along the stable halo orbits. In the poloidal plane, we also discuss shapes of the related effective potential halo lobes where the general off-equatorial motion can be bound. Then we focus on the halo orbits near a Kerr black hole immersed in an asymptotically uniform magnetic field of external origin.

We demonstrate that, in both the cases considered, the lobes exhibit two different regimes, namely, one where completely disjoint lobes occur symmetrically above and below the equatorial plane, and another where the lobes are joined across the plane. A possible application of the model concerns the structure of putative circumpulsar discs consisting of dust particles. We suggest that the particles can acquire a small (but non-zero) net electric charge, and this drives them to form the halo lobes.

PACS numbers: 04.25.-g, 04.40.Nr, 04.70.Bw, 04.90.+e

1. Introduction

Motion of matter near compact stars and black holes has been discussed thoroughly in textbooks [1, 2]. In the test-particle approximation, the hydrodynamical terms are neglected, as expected in circumstances when the medium is rarefied and the mean free path is comparable with the typical length-scale of the system [3–5]. The interplay between gravitational attraction and the electromagnetic attraction or repulsion is essential for characteristics of the motion, namely, its stability properties. Motivation for these studies arises from the problem of motion and acceleration of matter (charged particles or dust grains) [6–10].

Compact stars can be imagined as being endowed with magnetic dipoles that are anchored in the stars and co-rotate with them [6, 11, 12]. Rotation gives rise to the electric component of the field, and we assume that the resulting structure dominates over the small-scale turbulent fields. On the other hand, uncharged black holes do not support their own intrinsic magnetic fields; they can only be embedded in external fields [13, 14]. In general, the gravitational and electromagnetic fields interact with each other and the result is determined through the Einstein-Maxwell equations. To avoid such a complex description, one can also consider a test electromagnetic field influenced by the given gravitational field.

In both cases, magnetic compact stars as well as magnetized black holes‡, the interplay of strong gravity, rotation and magnetic field is capable of accelerating electrically charged particles and, possibly, it can also introduce new families of stable motion. The latter will be the main subject of the present paper.

Recently, we have studied the existence of stable circular orbits with fixed latitudes of charged particles moving off the equatorial plane (halo orbits) [15, 16]. We assumed an axially symmetric (aligned) magnetic dipolar field and built our discussion on classical studies [17, 18] derived in the context of weak (Newtonian) gravitational fields, and designed for planetary studies. Particles on halo orbits are bound to the central object by a combined effect of gravitational and electromagnetic forces and they do not have to cross neither the equatorial plane nor the rotation axis. In the poloidal plane, the halo orbits are located in a kind of lobes that are positioned symmetrically above and below the equatorial plane. The lobes may be disjoint or they may be interconnected, depending on the parameters. Our study [15], within the pseudo-Newtonian approach [19–21], has shown that the stable halo orbits can indeed emerge also near magnetic compact stars, where their structure is affected by strong gravitational field. We have also examined the case of charged and rotating (Kerr-Newman) black holes and naked singularities. Surprisingly, the stable halo orbits do not exist above the horizon of Kerr-Newman black holes. This suggests that the structure of the Kerr-Newman spacetime is in several aspects quite special one, while the generic case of dipole-type field usually allows for the motion along stable halo orbits.

‡ We use the term magnetic compact stars (magnetic stars) to specify neutron stars, Q-stars and hybrid stars as well, and the magnetized black holes for the black holes embedded in ordered magnetic fields.

Here, we extend our investigation of the halo orbits to the case of magnetic compact stars and magnetized black holes in general relativity. To this end, we study the existence and orientation of stable halo orbits which surround the minima of two-dimensional effective potential in the poloidal (r, θ)-plane. We also deal with qualitatively different cases of the general, in the halo lobes bounded, off-equatorial motion (halo motion). Namely, we point out to the motion in two separated halo lobes extending symmetrically above and below the equatorial plane versus the motion in a single region arising from the merged lobes across the equatorial plane. We also distinguish the cases when the halo lobes admit outflow of particles to the outer space or they allow the inflow onto the central body.

In the space environment, dust particles can carry small electrostatic charges [22]. An astrophysical motivation to study the halo motion of such weakly charged particles is the search for circumpulsar debris that could be formed from a fall-back disc resulting from the fraction of the explosion ejecta material that fails to escape [23–25]. The anomalous X-ray pulsars [26] represent a category of magnetars around which the infrared observation indicate the presence of debris dust discs, potentially relevant for our deliberation. These are young neutron stars in the category of magnetars with slow spin periods in a range $\approx$ 2–12 seconds. The minimum distance to which the dust can reach is uncertain, however, part of it may enter the magnetosphere and influence the current flows below the light cylinder, until the dust evaporates. The potential relevance of the halo motion of dust particles is based on the fact that these orbits occupy areas of the stable motion. The irradiated dust particles acquire a small net electric charge and modulate the source radiation at their characteristic oscillation frequencies as they move in the halo lobes.

The paper is organized as follows. In section 2, we combine the standard formulation based on the construction of the super-Hamiltonian and the corresponding effective potential, with perhaps a less frequent (in this context) formalism of forces in the projected three-space [27–30]. We maintain the assumption about axial symmetry but we generalise ref. [15] by considering the background of the magnetic compact star in a more consistent framework, i.e. in the Schwarzschild geometry with a test dipole-type rotating magnetic field [6] (section 3). Furthermore, as a qualitatively different situation, we also consider a rotating black hole immersed in the uniform magnetic field [14] (section 4). We discuss the astrophysical relevance in section 5 and then we conclude the paper in section 6.

2. Formalism

According to the standard approach to a test particle motion, we start by construction of the super-Hamiltonian [2]

$$\mathcal{H} = \tfrac{1}{2}\, g^{ij} \Big(\pi_i - \tilde{q} A_i\Big) \Big(\pi_j - \tilde{q} A_j\Big), \tag{1}$$

where m and $\tilde{q}$ are the rest mass and electric charge of the particle, π_i is the canonical momentum, and A_i denotes the vector potential related to the electromagnetic tensor by $F_{ij} = A_{j,i} - A_{i,j}$. The particle motion is governed by Hamilton's equations

$$\frac{\mathrm{d}x^i}{\mathrm{d}\lambda} = \frac{\partial \mathcal{H}}{\partial \pi_i}, \quad \frac{d\pi_i}{d\lambda} = -\frac{\partial \mathcal{H}}{\partial x^i}, \tag{2}$$

where $\lambda = \tau/m$ is the affine parameter and τ is the proper time.§ The first Hamilton's equation of motion implies

$$p^i \equiv \frac{\mathrm{d}x^i}{\mathrm{d}\lambda} = \pi^i - \tilde{q}A^i. \tag{3}$$

The second Hamilton's equation ensures that the generalized momenta,

$$\pi_t = p_t + \tilde{q}A_t \equiv -\tilde{E}, \quad \pi_\phi = p_\phi + \tilde{q}A_\phi \equiv \tilde{L}, \tag{4}$$

are constants of motion, reflecting the stationarity and axial symmetry of the system. These are connected with Killing vector fields $\eta^i = \delta^i_t$ and $\xi^i = \delta^i_\phi$.

We start by writing the normalization condition, $m^2 = -g^{ij}p_i p_j$, and defining the specific energy, angular momentum and charge, $E = \tilde{E}/m$, $L = \tilde{L}/m$ and $q = \tilde{q}/m$, respectively. We find the two-dimensional effective potential for the particle motion in the form [2]

$$V_{\text{eff}} = \frac{-\beta + (\beta^2 - 4\alpha\gamma)^{1/2}}{2\alpha}, \tag{5}$$

where

$$\alpha = -g^{tt}, \quad \beta = 2\Big[g^{t\phi}\Big(L - qA_\phi\Big) - g^{tt}qA_t\Big], \tag{6}$$

$$\gamma = -g^{\phi\phi}\Big(L - qA_\phi\Big)^2 - g^{tt}q^2A_t^2 + 2g^{t\phi}qA_t\Big(L - qA_\phi\Big) - 1, \tag{7}$$

reflecting the motion properties.

Alternatively to the Hamilton's equations (2), one can describe the motion by the Lorentz equation

$$u^k \nabla_k u^i = q\, F^i_k u^k. \tag{8}$$

For our purposes, we find this equation particularly well suited, when being rewritten in the formalism of forces [27]. The forces formalism is based on the projection $h_{ik} = g_{ik} + n_i n_k$ of the Lorentz equation (8) onto the three-dimensional hypersurface orthogonal to the four-velocity field of the Locally Non-Rotating Frames (LNRF) [31],

$$n^i = e^{-\Phi}(\eta^i + \Omega_{\text{LNRF}}\xi^i), \quad e^{2\Phi} = -(\eta^i + \Omega_{\text{LNRF}}\xi^i)(\eta^i + \Omega_{\text{LNRF}}\xi^i), \tag{9}$$

where the angular velocity $\Omega_{\text{LNRF}} = -g_{t\phi}/g_{\phi\phi}$. In the case of a static spacetime, $\Omega_{\text{LNRF}} = 0$ and the LNRF become static ones.

§ We use the geometric system of units ($c = G = 1$) and a positive signature of the metric. In order to reduce the number of parameters in our classification, we scale all quantities that have the dimension of the power of length by the mass M^* of the central object. In this way we adopt the scaled dimensionless quantities. Thus, our formulae become completely dimensionless. Furthermore, our attention is paid to the stationary and axially symmetric spacetimes, described by using the standard Boyer-Lindquist coordinates $x^i = (t, \phi, r, \theta)$, and endowed with the magnetic fields which adopt the same symmetries.

Let us consider an example of the halo motion – the circular motion at constant latitude θ (outside the equatorial plane). The four-velocity field of particles uniformly circling along the halo orbits can be decomposed as

$$u^i_{\rm h} = \gamma(n^i + v_{\rm h}\tau^i). \tag{10}$$

Here, $\gamma = (1 - v^2_{\rm h})^{-1/2}$ is the Lorentz factor, $\tau^i = \xi^i\, g_{\phi\phi}^{-1/2}$ is the unit spacelike vector orthogonal to n^i, along which the spatial velocity $v^i_{\rm h} = v_{\rm h}\tau^i$ is aligned. Both vectors in the decomposition (10) correspond to the base vectors of the standard orthonormal tetrad attached to LNRF: $n^i = e^i_{(t)}$ and $\tau^i = e^i_{(\phi)}$. Thus, $v_{\rm h}$ is the orbital (azimuthal) velocity measured with respect to LNRF.

Projection of the Lorentz equation, $h^k_j u^i \nabla_i u_k = q h^i_j F_{ik} u^k$, can be written in the form

$$\mathcal{G}_j + (\gamma v_{\rm h})^2 \mathcal{Z}_j + \gamma^2 v_{\rm h} \mathcal{C}_j = -q\gamma(\mathcal{E}_j + v_{\rm h}\mathcal{M}_j), \tag{11}$$

where the so-called mass and velocity independent parts of the gravitational, centrifugal and Coriolis inertial forces, and the charge and velocity independent parts of the electric and magnetic forces can be expressed as

$$\mathcal{G}_j = -\,\partial_j \Phi, \tag{12}$$

$$\mathcal{Z}_j = \tfrac{1}{2} g^{-1}_{\phi\phi}\, e^{-2\Phi}\Big(e^{2\Phi}\,\partial_j g_{\phi\phi} - g_{\phi\phi}\,\partial_j e^{2\Phi}\Big), \tag{13}$$

$$\mathcal{C}_j = g^{-3/2}_{\phi\phi}\, e^{-\Phi}\Big(g_{\phi\phi}\,\partial_j g_{t\phi} - g_{t\phi}\,\partial_j g_{\phi\phi}\Big), \tag{14}$$

$$\mathcal{E}_j = e^{-\Phi}\Big(\Omega_{\rm LNRF}\partial_j A_\phi + \partial_j A_t\Big), \tag{15}$$

$$\mathcal{M}_j = g^{-1/2}_{\phi\phi}\,\partial_j A_\phi, \tag{16}$$

where only the radial and latitudinal components are nonzero.

Our investigation of the existence and orientation of the stable halo motion is based on the following approach. First, we notice that loci of the halo orbits (stable as well as unstable) correspond to the stationary points of the effective potential (5). We are interested in the stable motion mainly, i.e. in those orbits which satisfy the conditions for the local minima of the potential,

$$\partial^2_r V_{\rm eff}(r, \theta; p, L_{\rm h}, q_{\rm h}) > 0, \tag{17}$$

$$\det {\rm H}(r, \theta; p, L_{\rm h}, q_{\rm h}) > 0. \tag{18}$$

Here, H is the Hessian matrix, p is a parameter characterizing the compact object (angular velocity Ω in the case of magnetic star, spin parameter a in the case of Kerr black hole), and $L_{\rm h}$ and $q_{\rm h}$ are the specific angular momentum and charge which are characteristic for a certain halo orbit.

According to the forces formalism, we can determine $L_{\rm h}$ and $q_{\rm h}$ from the balance equations‖

$$\mathcal{G}_r + (\gamma v_{\rm h})^2 \mathcal{Z}_r + \gamma^2 v_{\rm h} \mathcal{C}_r = -q_{\rm h}\gamma(\mathcal{E}_r + v_{\rm h}\mathcal{M}_r), \tag{19}$$

‖ Note that alternatively to equations (19)–(20), the specific angular momentum $L_{\rm h}$ and charge $q_{\rm h}$ can be determined also from the conditions $\partial_r V_{\rm eff} = 0$ and $\partial_\theta V_{\rm eff} = 0$. However, this routine is more complicated, especially in our second case of the Kerr black hole in the uniform magnetic field.

$$\mathcal{G}_\theta + (\gamma v_{\rm h})^2 \mathcal{Z}_\theta + \gamma^2 v_{\rm h} \mathcal{C}_\theta = -q_{\rm h}\gamma(\mathcal{E}_\theta + v_{\rm h}\mathcal{M}_\theta). \tag{20}$$

Eliminating $q_{\rm h}$ and assuming $0 < \theta < \pi$, $\theta \neq \pi/2$, we get the cubic equation

$$A v_{\rm h}^3 + B v_{\rm h}^2 + C v_{\rm h} + D = 0, \tag{21}$$

where

$$A = \mathcal{M}_\theta(\mathcal{G}_r - \mathcal{Z}_r) + \mathcal{M}_r(\mathcal{Z}_\theta - \mathcal{G}_\theta), \tag{22}$$

$$B = \mathcal{E}_r(\mathcal{G}_r - \mathcal{Z}_r) + \mathcal{E}_r(\mathcal{Z}_\theta - \mathcal{G}_\theta) + \mathcal{C}_\theta\mathcal{M}_r - \mathcal{C}_r\mathcal{M}_\theta, \tag{23}$$

$$C = \mathcal{C}_\theta\mathcal{E}_r - \mathcal{C}_r\mathcal{E}_\theta + \mathcal{G}_\theta\mathcal{M}_r - \mathcal{G}_r\mathcal{M}_\theta, \tag{24}$$

$$D = \mathcal{E}_r\mathcal{G}_\theta - \mathcal{E}_\theta\mathcal{G}_r. \tag{25}$$

The cubic equation (21) has in general three complex solutions,

$$v_{\rm h,i} = v_{\rm h,i}(r, \theta; p), \tag{26}$$

where $\mathrm{i} \in \{\mathrm{I}, \mathrm{II}, \mathrm{III}\}$. These can represent values of orbital velocities of the charged particles moving along the halo orbits. The corresponding specific charges can be derived from one of the equations (19)–(20). We find

$$q_{\rm h,i} = \frac{\mathcal{G}_r(v_{\rm h,i}^2 - 1) - v_{\rm h,i}\,(\mathcal{C}_r + v_{\rm h,i}\,\mathcal{Z}_r)}{(\mathcal{E}_r + v_{\rm h,i}\,\mathcal{M}_r)\left(1 - v_{\rm h,i}^2\right)^{1/2}}. \tag{27}$$

Finally, the three values of the specific angular momentum are

$$L_{\rm h,i} = \gamma\, v_{\rm h,i}\, g_{\phi\phi}^{1/2} + q_{\rm h,i}\, A_\phi. \tag{28}$$

Searching systematically through the parameter space $(r \times \theta \times p)$, we can now investigate the validity of conditions (17), (18) and $v_{\rm h,i} \in R$, $|v_{\rm h,i}| < 1$, necessary and sufficient for the existence of the stable halo orbits.

3. Magnetic star

To a good approximation, the gravitational field outside a compact star is described by Schwarzschild metric [2]

$$\mathrm{d}s^2 = -\left(1 - 2r^{-1}\right)\mathrm{d}t^2 + \left(1 - 2r^{-1}\right)^{-1}\mathrm{d}r^2 + r^2(\mathrm{d}\theta^2 + \sin^2\theta\mathrm{d}\phi^2). \tag{29}$$

Naturally, the gravitational field of rotating compact star differs from the Schwarzschild metric (in the case of slow rotation it is well determined by the Hartle-Thorne metric [32]). However, one does not need to consider this discrepancy, taking advantage of the simple analytical form of the Schwarzschild metric element that captures the essential properties of the motion not only near non-rotating black holes, but above the surface of ultra-compact stars and farther away from slowly rotating black holes as well. The test dipole magnetic field rotating with angular velocity Ω in the Schwarzschild geometry can be expressed in terms of the vector potential [6]

$$A_t = \tfrac{3}{8}\Omega\mathcal{M}\mathcal{R}\sin^2\theta, \quad A_\phi = -\tfrac{3}{8}\mathcal{M}\mathcal{R}\sin^2\theta, \tag{30}$$

where

$$\mathcal{R} = 2 + 2r + r^2\ln\left(1 - 2r^{-1}\right). \tag{31}$$

The related dipole magnetic moment is [33]

$$\mathcal{M} = \frac{4R^{3/2}\,(R-2)^{1/2}}{6(R-1)+3R\,(R-2)\,\ln\left(1-2R^{-1}\right)}\,B_0. \tag{32}$$

This configuration can be considered as a model of magnetic compact star (radius R and angular velocity Ω) endowed with an aligned co-rotating magnetic field of strength B_0. The latter is measured with respect to the standard orthonormal tetrad of static observers on the surface of the star in the equatorial plane. Rotation terms are neglected in the metric and the frozen-in condition for the magnetic field is imposed, $F^i_j\,u^j_{\rm MF}=0$ (force-free approximation), where $u^i_{\rm MF}=(u^t_{\rm MF},u^\phi_{\rm MF},0,0)$, i.e. $u^\phi_{\rm MF}/u^t_{\rm MF}=\Omega$.

Employing equations (29) and (30), the effective potential (5) adopts the form

$$\begin{aligned} V_{\rm eff} = & -\tfrac{3}{8}\,q\mathcal{M}\Omega\mathcal{R}\sin^2\theta \\ & +\left(1-2r^{-1}\right)^{1/2}\left[1+\left(\frac{L}{r\sin\theta}+\frac{3q\mathcal{M}\mathcal{R}\sin\theta}{8r}\right)^2\right]^{1/2}. \end{aligned} \tag{33}$$

The only restriction following from the potential formula is $r>2$ (event horizon). However, the effective potential is not meaningful outside the region between the considered surface of the star and the light cylinder, arising due to the condition $g_{ik}u^i_{\rm MF}u^k_{\rm MF}<0$, thus being implicitly defined by the formula

$$\Omega^2 r_{\rm lc}^3\sin^2\theta_{\rm lc}-r_{\rm lc}+2=0. \tag{34}$$

Table 1. Signs of quantities characterizing the motion along stable halo orbits. Values of r and Ω are taken from the specific regions corresponding to figure 1.

Reg.	$v_{\rm h,I}$	$Q_{\rm h,I}$	$L_{\rm h,I}$	Reg.	$v_{\rm h,II}$	$Q_{\rm h,II}$	$L_{\rm h,II}$	Reg.	$v_{\rm h,III}$	$Q_{\rm h,III}$	$L_{\rm h,III}$
A	+	−	+	A′	−	+	−	C	+	+	+
B	+	−	+	B′	−	+	−	C′	−	−	−

3.1. Existence and orientation of halo orbits

The general analysis in section 2 demonstrated that the dipole magnetic field (30) in the Schwarzschild geometry (29) allows for the existence of the stable halo orbits. We took advantage of the fact that q appears in all formulae as a product with $\mathcal{M}$, so we could introduce the effective specific charge $Q=q\mathcal{M}$ instead of the usual specific charge q. This decreases the number of parameters. Only the parameter $p\equiv\Omega$ remains in the relations for $v_{\rm h,i}$ (26), $L_{\rm h,i}$ (28) and $Q_{\rm h,i}$, being expressed by the same formula as $q_{\rm h,i}$ (27).

The following conclusions about the existence of stable halo orbits arise from figure 1. The stable halo orbits are possible for particles which co-rotate with the dipole and whose charge satisfies either the condition $Q_{\rm h}\Omega<0$ (regions A, B′) or $Q_{\rm h}\Omega>0$ (regions C, C′). By co-rotation of particles we mean $v_{\rm h}\Omega>0$, i.e. $\mathrm{sgn}(v_{\rm h})=\mathrm{sgn}(\Omega)$. Particles can also counter-rotate with the dipole along stable halo orbits; in such case

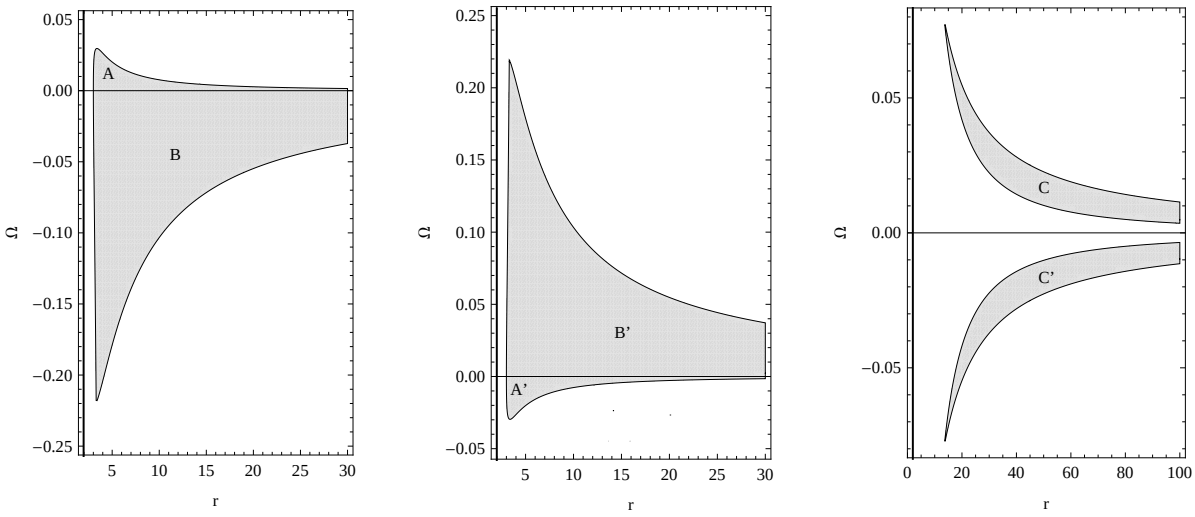

Figure 1. The range and orientation of particle motion along stable halo orbits near a magnetic star. The star rotates with angular velocity Ω. This figure has been constructed for the latitude $\theta = \pi/3$ and it represents a typical result for the effective potential $V_{\rm eff}(r,\theta;L,Q,\Omega)$, based on the behaviour of three orbital velocities $v_{\rm h,I}(r,\theta;\Omega)$, $v_{\rm h,II}(r,\theta;\Omega)$ and $v_{\rm h,III}(r,\theta;\Omega)$ (roots of equation (21)). These correspond to the specific angular momenta $L_{\rm h,I}(r,\theta;\Omega)$, $L_{\rm h,II}(r,\theta;\Omega)$, $L_{\rm h,III}(r,\theta;\Omega)$ and the effective specific charges $Q_{\rm h,I}(r,\theta;\Omega)$, $Q_{\rm h,II}(r,\theta;\Omega)$, $Q_{\rm h,III}(r,\theta;\Omega)$. The gray areas correspond to the parameters for which the effective potentials $V_{\rm eff}(r,\theta;L_{\rm h,I},Q_{\rm h,I},\Omega)$ (left panel), $V_{\rm eff}(r,\theta;L_{\rm h,II},Q_{\rm h,II},\Omega)$ (middle panel) and $V_{\rm eff}(r,\theta;L_{\rm h,III},Q_{\rm h,III},\Omega)$ (right panel) develop local minima. Only the regions under the light cylinder are considered. The thick vertical lines denote position of the event horizon at $r = 2$. Description of the regions is summarized in table 1.

the charge must satisfy the condition $Q_{\rm h}\Omega > 0$ (regions A′, B). Thus, in the case of the same orientation of the magnetic dipole and its rotation ($\mathcal{M}\Omega > 0$), negatively charged particles moving along stable halo orbits can only co-rotate, whereas positively charged particles can either co-rotate or counter-rotate with the dipole.

We point out that the above-mentioned results are general. Qualitatively the same structure appears at any latitude, $0 < \theta < \pi$, $\theta \neq \pi/2$ (the assumption of $\theta = \pi/3$ in the figure 1 is not crucial). Note that $v_{\rm h}L_{\rm h} > 0$ holds always for every stable halo orbit.

3.2. Effective potential and classification of halo motion

As we can conclude from equation (33), the effective potential is invariant under combinations of simultaneous sign reversals maintaining

$$\mathrm{sgn}(Q\,\Omega) = \mathrm{const}, \quad \mathrm{sgn}(\Omega L) = \mathrm{const}. \tag{35}$$

At the event horizon, the potential diverges as

$$\lim_{r\to+2} V_{\rm eff} = \mathrm{sgn}(\mathrm{Q}\,\Omega)\infty. \tag{36}$$

In the non-rotating case, the effective potential is invariant under the signs reversals which satisfy

$$\mathrm{sgn}(QL) = \mathrm{const}. \tag{37}$$

The effective potential (33) exhibits a rich spectrum of behaviour. Different topology of the effective potential determines different possible regimes of charged particles motion and yields the following classification. Note that locations of the surface of the star and of the light cylinder must be incorporated into the classification as well. For instance, with respect to the different positions of the light cylinder, we obtain an additional type IIIa′ to the type IIIa (although the behaviour of the potential itself is identical in both the cases). Similarly, different positions of the surface of the star bring the additional type Ia′ to the type Ia, and the type IIb′ to the type IIb. On the other hand, the different types of the potential behaviour itself do not have to enrich the considered classification necessarily. For example, the different number of saddle points that occur below the star surface or beyond the light cylinder does not influence the topology between surface of the star and light cylinder, and is irrelevant for us.

The family of different types of the effective potential can be parameterized by (conserved) energy of the moving particle. Starting at the energy corresponding to local minima of the potential and rising gradually the energy level (and keeping the other parameters constant), we first observe the gradually growing lobes of halo orbits, where particles are trapped. The following classification emerges (see figures 2–3).¶

Type Ia. Halo lobes merge together once the energy level of the saddle point in the equatorial plane is reached; particles moving within these merged lobes can cross the equatorial plane. Later, when the energy is high enough, particles start falling onto the surface of the magnetic star in the regions where the merged potential lobes open, and the particles hit the surface of the star. Increasing the energy further, the merged lobes open out also on the outer side, crossing the light cylinder. This way the particles can scatter away from the system.

Type Ib. Halo lobes merge through saddle points out of the equatorial plane. When the energy is high enough, the merged lobes open out through the surface of the star, and then also through the light cylinder.

Type IIa. Halo lobes merge through the saddle point in the equatorial plane. Then again, the merged halo lobes open out through the light cylinder and, finally, through the surface of the star.

¶ Because of the complex spectrum of the different types, we present only the most representative cases in the following list.

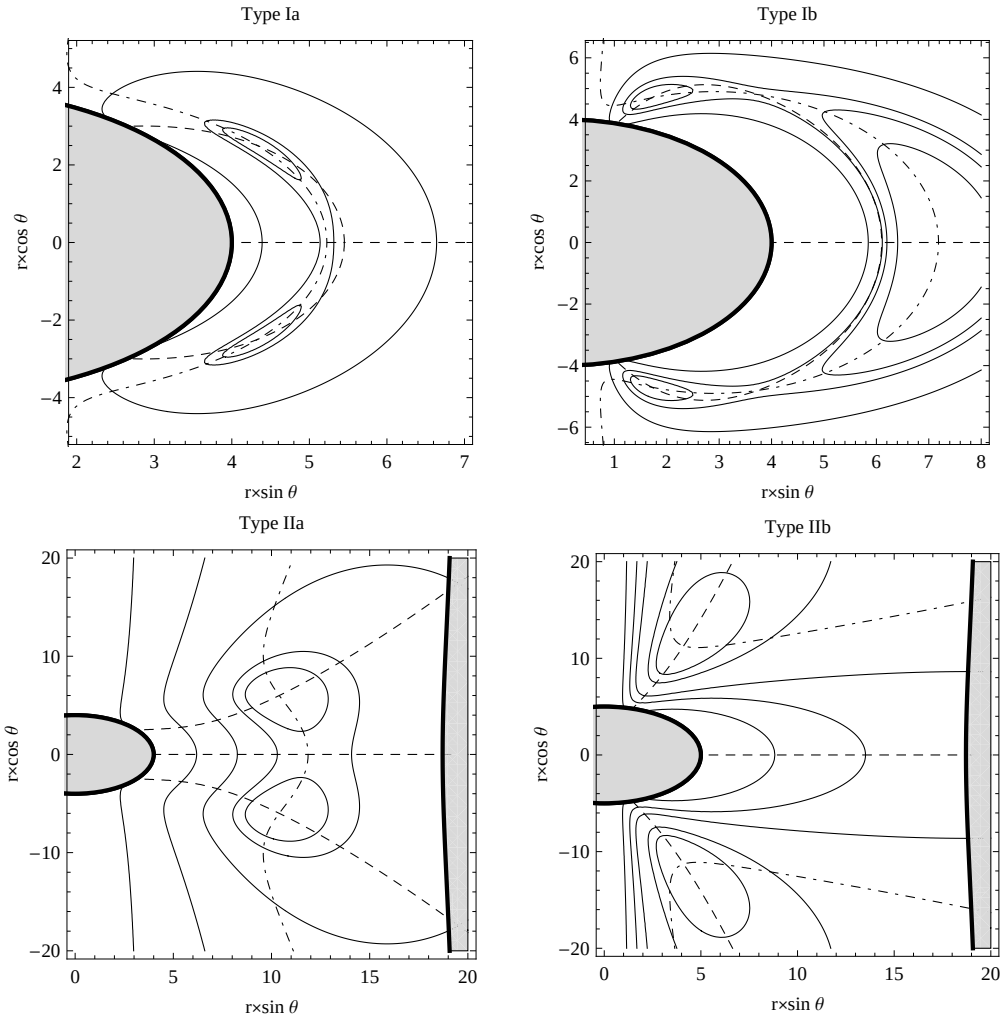

Figure 2. Behaviour of effective potential $V_{\rm eff}$ for charged particles moving near magnetic star. Qualitatively different types of behaviour of the effective potential occur, with two local minima in the poloidal plane. The lobes are limited by the radius of the star and the light cylinder (thick curves limiting the gray areas). The equipotential surfaces are shown by solid curves, whereas the dot-and-dashed and dashed lines correspond to zeroes of $\partial_r V_{\rm eff}$ and $\partial_\theta V_{\rm eff}$, respectively. The presented types correspond to the following combinations of parameters: **Ia**: $Q \doteq -5.72$, $L \doteq 0.876$, $\Omega \doteq 0.0115$, $R = 4$ and $\theta_{\rm h} = \pi/3, r_{\rm h} = 5$ (parameters taken from region A in figure 1); **Ib**: $Q \doteq -14.6$, $L \doteq 0.343$, $\Omega = 0.03$, $R = 4$ and $\theta_{\rm h} = \pi/9, r_{\rm h} = 5$; **IIa**: $Q \doteq 5.77$, $L \doteq -2.30$, $\Omega = 0.0505$, $R = 4$ and $\theta_{\rm h} = \pi/3, r_{\rm h} = 12$ (parameters taken from region B′ in figure 1); **IIb**: $Q \doteq 25.2$, $L \doteq -0.788$, $\Omega = 0.0505$, $R = 5$ and $\theta_{\rm h} = \pi/9, r_{\rm h} = 12$.

Type IIb. Halo lobes open out through the light cylinder. When the energy is high enough, the halo lobes merge through the saddle point located beyond the light cylinder. Increasing the energy further, the opened and merged lobes open out through the surface of the star.

Type IIIa. Halo lobes merge through the saddle point in the equatorial plane. Later, when the energy is high enough, the merged lobes open out through another saddle

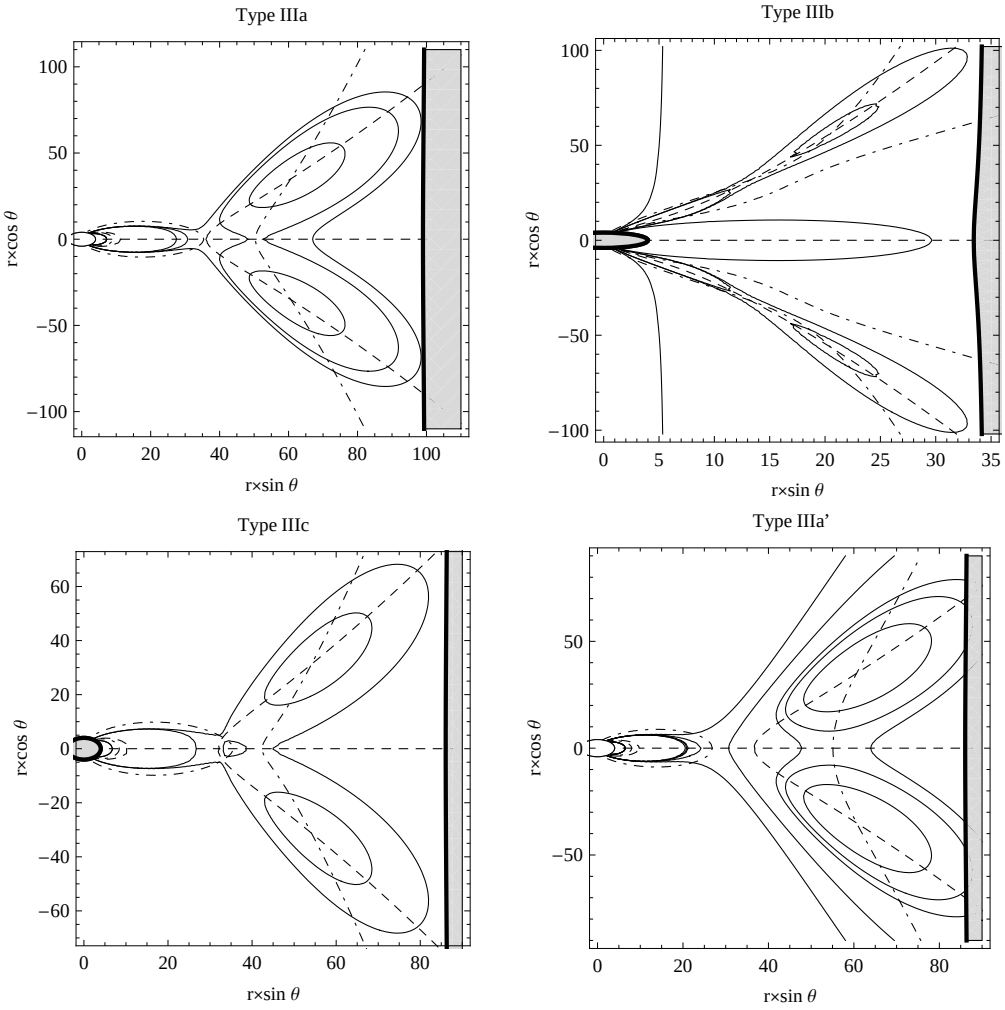

Figure 2. (Continued.) The presented types correspond to the following parameters: **IIIa**: $Q \doteq 53.4$, $L \doteq 6.58$, $\Omega = 0.01$, $R = 4$ and $\theta_{\rm h} = \pi/3, r_{\rm h} = 70$ (parameters taken from region C in figure 1); **IIIb**: $Q \doteq 113$, $L \doteq 2.43$, $\Omega = 0.029$, $R = 4$ and $\theta_{\rm h} = \pi/9, r_{\rm h} = 60$; **IIIc**: $Q \doteq 45.9$, $L \doteq 6.25$, $\Omega \doteq 0.0115$, $R = 4$ and $\theta_{\rm h} = \pi/3, r_{\rm h} = 62.5$ (parameters taken from region C in figure 1); **IIIa′**: $Q \doteq 44.5$, $L \doteq 6.50$, $\Omega = 0.0115$ and $\theta_{\rm h} = \pi/3, r_{\rm h} = 70$.

point in the equatorial plane. Finally, the lobes open through the light cylinder.

Type IIIb. Halo lobes open through saddle points out of the equatorial plane, and later, when the energy is high enough, through the light cylinder as well. The opened halo lobes merge through the saddle point in the equatorial plane hidden beyond the light cylinder.

Type IIIc. Halo lobes open out through saddle points out of the equatorial plane and merge this way with each other. Later, another corridor between the lobes emerges through the saddle point in the equatorial plane. The potential barrier between the saddle points can be overcome after increasing the energy further. Finally, the merged

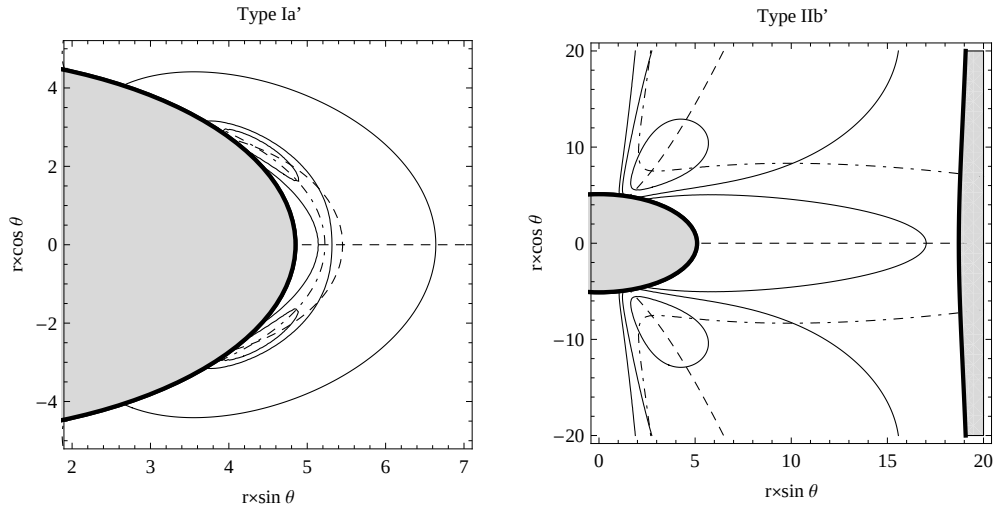

Figure 2. (Continued.) The presented types correspond to the following parameters: **Ia′**: $Q \doteq -5.72$, $L \doteq 0.876$, $\Omega \doteq 0.0115$, $R = 4.85$ and $\theta_{\rm h} = \pi/3, r_{\rm h} = 5$ (parameters taken from region A in figure 1); **IIb′**: $Q \doteq 17.1$, $L \doteq -0.617$, $\Omega = 0.0505$, $R = 5.1$ and $\theta_{\rm h} = \pi/9, r_{\rm h} = 8$.

and opened lobes open out through the light cylinder.

Type IIIa′. Halo lobes open out through the light cylinder. Later the opened lobes merge through the saddle point in the equatorial plane. Finally, increasing the energy more, the opened and merged lobes open out through the second saddle point in the equatorial plane.

Type Ia′. Halo lobes open out through the surface of the star, then the halo lobes merge through the saddle point in the equatorial plane, and, finally, by increasing the energy the lobes open out through the light cylinder.

Type IIb′. Halo lobes open out through the surface of the star, and later, when the energy is high enough, through the light cylinder. Increasing the energy further more, the opened lobes merge through the saddle point in the equatorial plane hidden beyond the light cylinder.

3.3. Features of the classification

In the case of parallel orientation of the rotation and the magnetic moment of the dipole, the behaviour of the potential of the types Ia, Ib and Ia′ (serie I) determine the motion of negatively charged particles which co-rotate along the stable halo orbits. At the event horizon, the potential diverges as $V_{\rm eff} \to -\infty$, and there are two additional saddle points of the potential near the event horizon (hidden under the surface of the star). In the equatorial plane, the effective potential develops local maxima (also hidden under the surface of the star) in addition to the saddle point. Note that the extent of halo lobes

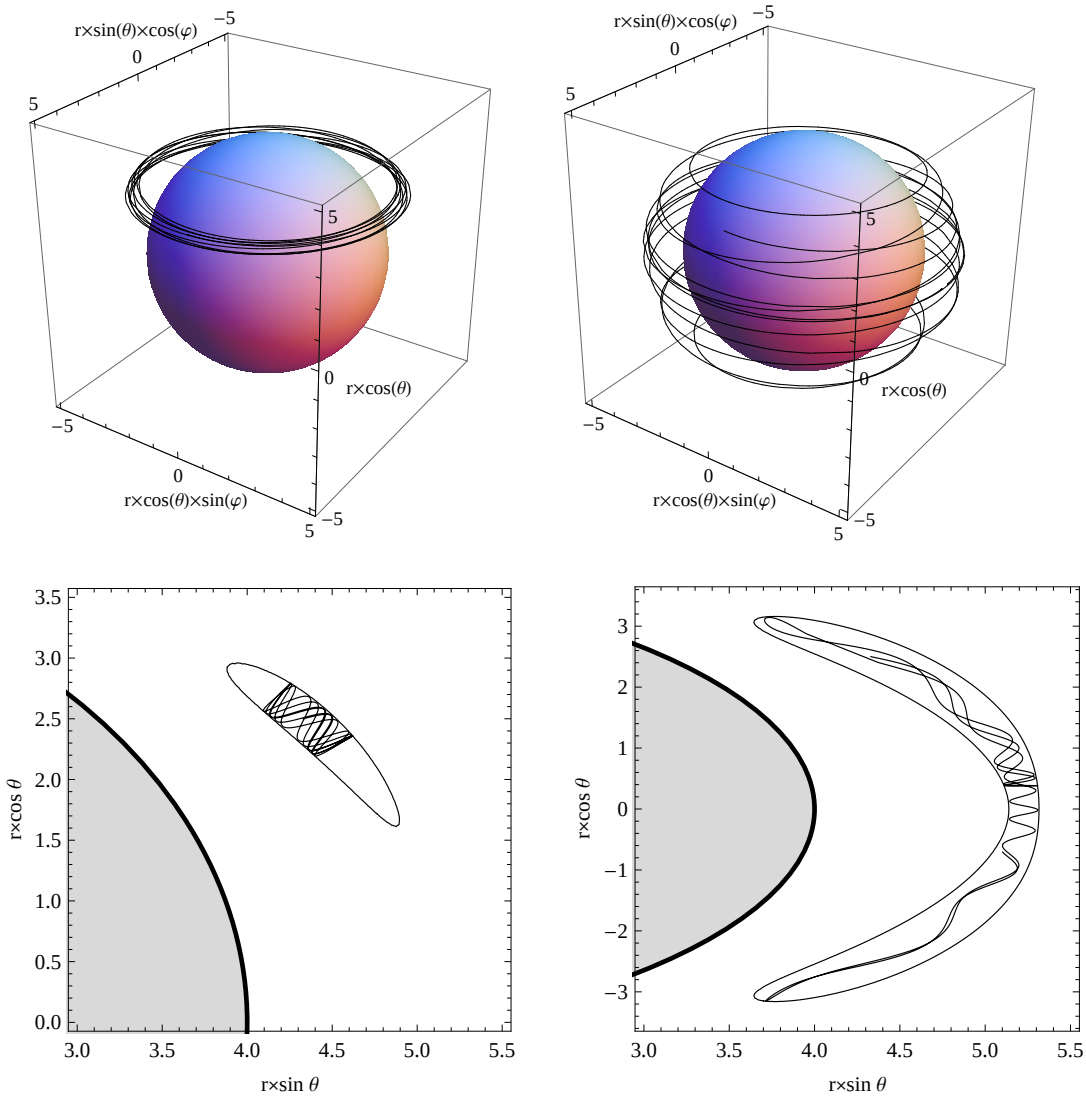

Figure 3. Three-dimensional trajectories of charged particles (upper panels) with $Q \doteq -5.72$ and the corresponding poloidal projection of the motion (lower panels), moving in the separated and merged halo lobes in the vicinity of a magnetic star with $R = 4$ and $\Omega \doteq 0.0115$. The trajectories were calculated numerically by using the Lorentz equation of motion (8) with the initial conditions $L \doteq 0.876$, $\phi(0) = 0$, $r(0) = 5$, $\theta(0) = \pi/3$, and $E = 0.8481$, $u^\theta(0) = 7 \times 10^{-4}$, $u^r(0) \doteq 0.021$ (motion in separated halo lobe), and $E = 0.8485$, $u^\theta(0) = 7 \times 10^{-3}$, $u^r(0) \doteq 0.020$ (motion in merged lobes).

can never be large (compared to the radius of the black hole horizon) and they cannot be placed farther off the star surface.

Behaviour of the types IIa, IIb and IIb′ (serie II) determines the motion of positively charged particles, counter-rotating along halo orbits. At the event horizon, the potential diverges as $V_{\rm eff} \to \infty$, and there are no other stationary points hidden under the surface of the star, neither out of the equatorial plane nor within the plane. A relatively high potential barrier develops between the halo lobes and the star. Now, the halo lobes can

be of large extent and they can be placed farther away from the star surface.

Finally, the behaviour of types IIIa, IIIb, IIIc and IIIa′ (serie III) determines the motion of positively charged particles, co-rotating along halo orbits. At the event horizon, the potential diverges as $V_{\rm eff} \to \infty$, and there are no other stationary points out of the equatorial plane. However, in the equatorial plane, the behaviour of the potential is more complicated. In some cases, there can be even more than four stationary points.

There is an infinite potential barrier at the event horizon in the types of series II and III, and behaviour of the potential closer to the magnetic star can be complicated, especially in types of the serie III. But having the sufficiently high energy, particles can always fall onto the star surface, for the star surface always takes place above the event horizon.

The types Ia, IIa, Ia′, IIIa and IIIa′ are characteristic for the 'lower' stable halo orbits, taking place near the equatorial plane. On the other hand, the types Ib, IIb and IIIb are characteristic for the 'upper' stable halo orbits which occur near the rotation axis. Behaviour of the type IIIc represents an intermediate situation.

4. Kerr black hole in uniform magnetic field

In order to incorporate the large scale magnetic field in our considerations, we employ Wald's test-field solution [14]. The electromagnetic field is given in terms of the vector potential

$$A_t = \tfrac{1}{2}\, B_0 \Big(g_{t\phi} + 2a\, g_{tt} \Big) - \tfrac{1}{2}\, \mathcal{Q}\, g_{tt} - \tfrac{1}{2}\, \mathcal{Q}, \tag{38}$$

$$A_\phi = \tfrac{1}{2}\, B_0 \Big(g_{\phi\phi} + 2a\, g_{t\phi} \Big) - \tfrac{1}{2}\, \mathcal{Q}\, g_{t\phi}, \tag{39}$$

in the background of Kerr metric

$$\begin{aligned} {\rm d}s^2 = & -\frac{\Delta}{\Sigma}\Big({\rm d}t - a\sin\theta\, {\rm d}\phi \Big)^2 + \frac{\sin^2\theta}{\Sigma}\Big[\left(r^2 + a^2\right)\, {\rm d}\phi - a\, {\rm d}t \Big]^2 \\ & + \frac{\Sigma}{\Delta}\, {\rm d}r^2 + \Sigma\, {\rm d}\theta^2, \end{aligned} \tag{40}$$

where $\Delta = r^2 - 2r + a^2$, $\Sigma = r^2 + a^2 \sin^2\theta$ (a is the rotational parameter). $\mathcal{Q}$ stands for the test charge of the black hole; the terms containing $\mathcal{Q}$ may be identified with the components of vector potential of the Kerr-Newman solution [2]. Further, the asymptotic behaviour of components (38)–(39) justifies the identification of the parameter B_0 with the strength of the uniform magnetic field into which the Kerr black hole has been immersed. Wald [14] has shown that in the case of parallel orientation of the spin and the magnetic field B_0, the black hole selectively accretes positive charges (negative for the antiparallel orientation) until it is charged to the equilibrium value

$$\mathcal{Q}_{\rm W} = 2B_0\, a. \tag{41}$$

We will adopt $\mathcal{Q}_{\rm W}$ as a preferred value of the charge in forthcoming examples.

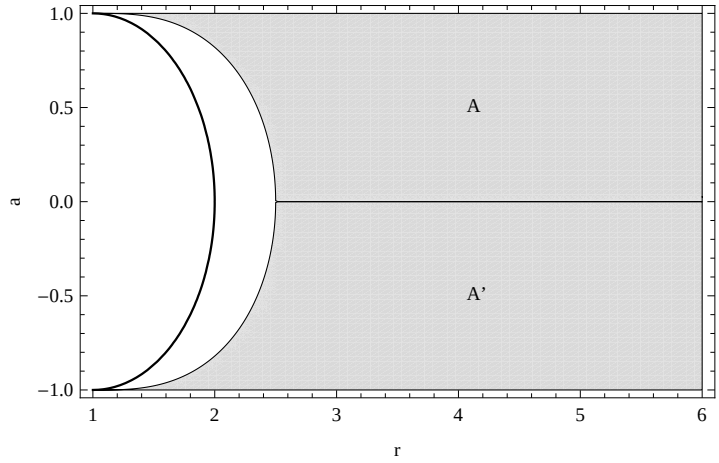

Figure 4. The range and orientation of particle motion along stable halo orbits near a Kerr black hole (with the spin a) embedded in a uniform magnetic field. This figure has been constructed for the latitude $\theta = \pi/3$ and it represents a typical result for the effective potential $V_{\rm eff}(r, \theta; L, Q, a)$ based on the investigation of the orbital velocity $v_{\rm h,I}(r, \theta; a)$ (root of equation 21 with $A = 0$). The corresponding specific angular momenta and charges are $L_{\rm h,I}(r, \theta; a)$ and $Q_{\rm h,I}(r, \theta; a)$. The gray regions correspond to the the local minima of the effective potential $V_{\rm eff}(r, \theta; L_{\rm h,I}, Q_{\rm h,I}, a)$. The thick solid curve shows the position of the event horizon at $r = 1 + (1 - a^2)^{1/2}$. Further classification is given in table 2.

Table 2. Signs of quantities characterizing the motion along stable halo orbits. Values of r and a are taken from the specific regions corresponding to figure 4.

Reg.	$v_{\rm h,I}$	$Q_{\rm h,I}$	$L_{\rm h,I}$
A	$-$	$+$	$+$
A′	$+$	$-$	$-$

4.1. Existence and orientation of halo orbits

Our analysis was described in general in section 2. Its application to the case of Wald's test-field is shown in figure 4. Again, we take the advantage of the fact that q appears only in the product with B_0, which leads us to introduce the effective specific charge $Q = qB_0$. Then, the only parameter $p \equiv a$ remains in the relations for $v_{\rm h,i}$ (26), $L_{\rm h,i}$ (28) and $Q_{\rm h,i}$ being expressed by the same formula as $q_{\rm h,i}$ (27). Note that due to the use of Wald's charge, the coefficient A in equation (21) vanishes. Moreover, having now the quadratic equations, one of the two possible roots does not take the real values from the interval $(-1, 1)$ in the considered black hole region above the outer event horizon. Thus, there is only one possible root $v_{\rm h,I}(r, \theta; a)$ and the related specific angular momentum $L_{\rm h,I}(r, \theta; a)$ and effective specific charge $Q_{\rm h,I}(r, \theta; a)$ involved in the classification routine.

In the region above the outer event horizon, the stable halo orbits are possible only for particles which counter-rotate with respect to LNRF ($v_{\rm h} a < 0$) and charge of which satisfies the condition $Q_{\rm h} a > 0$ (regions A, A′). The parallel orientation of the

spin a and the magnetic field B_0 ($aB_0 > 0$) allows counter-rotation along stable halo orbits only for positively charged particles. Moreover, in the potential minimum, there is always $v_{\rm h}L_{\rm h} < 0$.

4.2. Effective potential and classification of halo motion

We can conclude from formulae (40), (5), (38) and (39) that the potential $V_{\rm eff}$ allows several combinations of simultaneous sign reversals which follow from its symmetries. These have to satisfy the conditions

$$\mathrm{sgn}(Qa) = \mathrm{const}, \quad \mathrm{sgn}(aL) = \mathrm{const}. \tag{42}$$

The effective potential (5) does not reveal as many possibilities of stable halo motion as we have seen in the previous case of a magnetic star in section 3.2. Moreover, here, only the topology of the potential is crucial for the classification of the halo motion. Starting at energy of the potential local minima and rising its level (keeping other parameters constant), we still observe the growing halo lobes in which particles are trapped. The system can be classified in the following way (see figure 5).

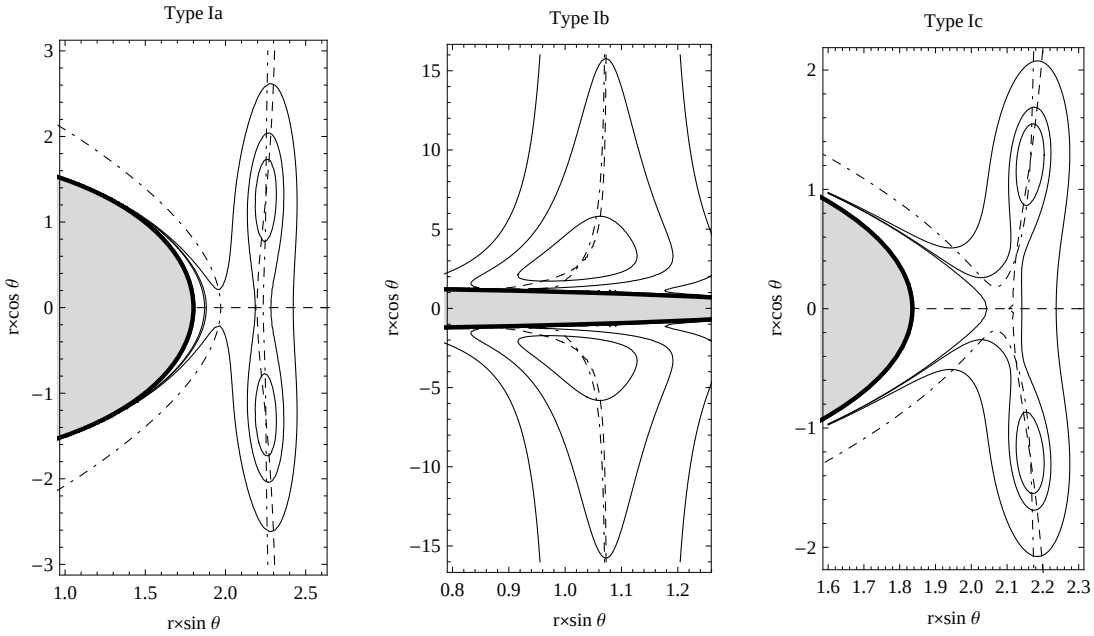

Figure 5. Behaviour of the effective potential $V_{\rm eff}$ for charged particles moving near Kerr black hole in the uniform magnetic field. These are typical examples of behaviour of the potential with two potential minima, again introduced in terms of the equipotential surfaces. The dashed and dot-and-dashed curves correspond to zeros of $\partial_\theta V_{\rm eff}$ and $\partial_r V_{\rm eff}$, respectively. The gray region corresponds to the interior of black hole, limited by the outer event horizon. The presented types correspond to the following parameters: **Ia**: $Q \doteq 1.37$, $L \doteq 3.76$, $a = 0.6$ and $\theta_{\rm h} = \pi/3, r_{\rm h} = 2.6$; **Ib**: $Q \doteq 4.79$, $L \doteq 2.76$, $a = 0.9$ and $\theta_{\rm h} = \pi/9, r_{\rm h} = 3$; **Ic**: $Q \doteq 1.60$, $L \doteq 4.02$, $a = 0.55$ and $\theta_{\rm h} = \pi/3, r_{\rm h} = 2.5$. The parameters of all the presented types are taken from the region A in figure 4.

Type Ia. Halo lobes merge with each other when the energy level is reached of the saddle point in the equatorial plane. Particles moving in these merged lobes can cross the equatorial plane. When the energy is increased high enough, particles can fall into the black hole, passing the next saddle point in the equatorial plane, through which the merged halo lobes open out.

Type Ib. Halo lobes open out through the saddle points out of the equatorial plane and the trapped particles can fall into the black hole.

Type Ic. Halo lobes merge through two saddle points out of the equatorial plane and they open out this way. Trapped particles can cross the equatorial plane or fall into the black hole.

In the case of the parallel orientation of the spin and the magnetic field, the behaviour of all the presented types determines the motion of positively charged particles counter-rotating along the stable halo orbit. The behaviour of type Ia is characteristic for potentials determining the 'lower' stable halo orbits. Type Ib is characteristic for the potential determining the 'upper' stable halo orbits. Type Ic exhibits an intermediate type.

In all the presented results here, we assume $\mathcal{Q} = 2B_0a$. But we checked that the stable halo orbits are also possible in the uncharged case, $\mathcal{Q} = 0$, finding no substantial change in the topology of effective potential compared to the charged case.

5. Discussion: The astrophysical relevance of halo orbits

In this paper, we have concentrated ourselves on aspects of the off-equatorial motion near magnetic compact stars and magnetized black holes. Namely, we discussed the existence of halo orbits, classified them into several categories and investigated their dependence on the parameters. Despite the obvious limitations of our approach, one can recognize several astrophysically relevant features of the halo orbits.

We can list the main limitations of the present approach: (i) Test-particle approximation was employed. This assumes that the medium is highly diluted and the mean free path is comparable with the characteristic size of the system (gravitational radius of the black hole). (ii) Schwarzschild metric was adopted for the external gravitational field of the magnetic compact star and Kerr metric for the rotating black hole, ignoring all other terms that could contribute to the gravitational field. Such contributions could in principle originate from the internal structure of the star and its rotation, or they could be caused by accreted matter outside the central body. (iii) The rotating dipole or the asymptotically uniform structure has been imposed as two examples of the magnetic field and the associated electric field. It was also assumed that the electromagnetic field does not affect the spacetime metric, so it could be treated in the test-field approximation.

The assumptions (ii) and (iii) are less critical because they are well fulfilled under the typical astrophysical conditions. We considered two different examples of the magnetic and gravitational fields, we found that the halo orbits are possible in both. The halo orbits are determined by their location in the poloidal (r,θ) plane, and by values of other parameters, such as the magnetic field strength and the specific charge of the particles. The assumption (i) is the crucial one and it imposes the main restriction on the choice of the system which can be described.

As for the numerical values of the mass-scaled (dimensionless) parameters Ω, a and Q, we can check the adequate choice by looking at the domain of the non-scaled quantities $\Omega^* = \Omega/M^*$, $a^* = aM^*$, $B_0^* = B_0/M^*$, $q^* = q$, $R^* = RM^*$ and M^*, characterizing real objects.

5.1. Magnetic star

In the following analysis, we assume masses and radii of magnetic compact stars in the ranges $1\,\mathrm{M}_\odot \leq M^* \leq 3\,\mathrm{M}_\odot$ and $3M^* \leq R^* \leq 10M^*$ [34], and magnetic fields and rotation frequencies reaching $B_0^* = 10^{10}\,\mathrm{T}$ and $f^* = 10^3\,\mathrm{Hz}$ ($\Omega^* \doteq 6283\,\mathrm{rad/s}$) [35–37].[+]

The limits of the used scaled parameters can be determined from the figure 6, which can be read in the following way. In the upper left plot, starting from the assumed astrophysically relevant values of angular velocity $\Omega^* \leq 10^{3.8}$, we can determine values of Ω for a fixed mass M^*. For example, light magnetic compact stars with $M^* = 1\,\mathrm{M}_\odot$ can rotate with the scaled angular velocity up to $\Omega \doteq 0.031$, while the heavy ones with $M^* = 3\,\mathrm{M}_\odot$ up to $\Omega \doteq 0.093$. In the upper right plot, within the astrophysically relevant values of magnetic field strength $B_0 \leq 10^{10}$, we can determine values of B_0 for a fixed mass M^*.* We notice that light magnetic compact stars with $M^* = 1\,\mathrm{M}_\odot$ can be endowed with magnetic fields of the scaled strength up to $B_0 \doteq 10^{-5.4}$, while the heavy ones with $M^* = 3\,\mathrm{M}_\odot$ up to $B_0 \doteq 10^{-4.9}$. In the lower left plot, for the scaled magnetic field strength $B_0 \leq 10^{-4.9}$, we can determine values of $\mathcal{M}$ for a fixed scaled radius R. We can also see that small magnetic compact stars with $R = 3$ allow scaled magnetic dipole momenta up to $\mathcal{M} \doteq 10^{-3.9}$, while the large ones with $R = 10$ up to $\mathcal{M} \doteq 10^{-2.0}$. In the lower right plot, for the specific charges $q \leq 10^{21}$, we can determine values of Q for a fixed magnetic dipole moment $\mathcal{M}$. Note that small scaled magnetic dipole momenta of $\mathcal{M} = 10^{-15}$ allow effective specific charges up to $Q = 10^6$, while the big ones of $\mathcal{M} = 10^{-2}$ can support values up to $Q = 10^{19}$.

[+] The precise determination of the mentioned limits is still of high interest, being very complex, dependent on the considered equation of state, etc. Moreover, not all the theoretical calculated models have their observable counterparts. For instance, as for the masses of neutron stars, the narrower range $1.4\,\mathrm{M}_\odot \lesssim M^* \lesssim 2.5\,\mathrm{M}_\odot$ is widely stated for the astrophysically relevant neutron stars. As for the radii, most of the realistic equations of state imply the lower limit only $R^* \approx 3.5M^*$ [38]. On the other hand, the existence of extremely compact stars with $R^* < 3M^*$ is also discussed. Some models for the so-called Q-stars allow the lower limit even $R^* \approx 2.8M^*$ [39–41]. In this paper, the limits are considered only for order estimates of the used dimensionless parameters, thus their exact values are of less importance here.

* The value of Ω^* is in physical (SI) units, i.e. rad/s. Similarly, B_0^* is expressed in units of Tesla.

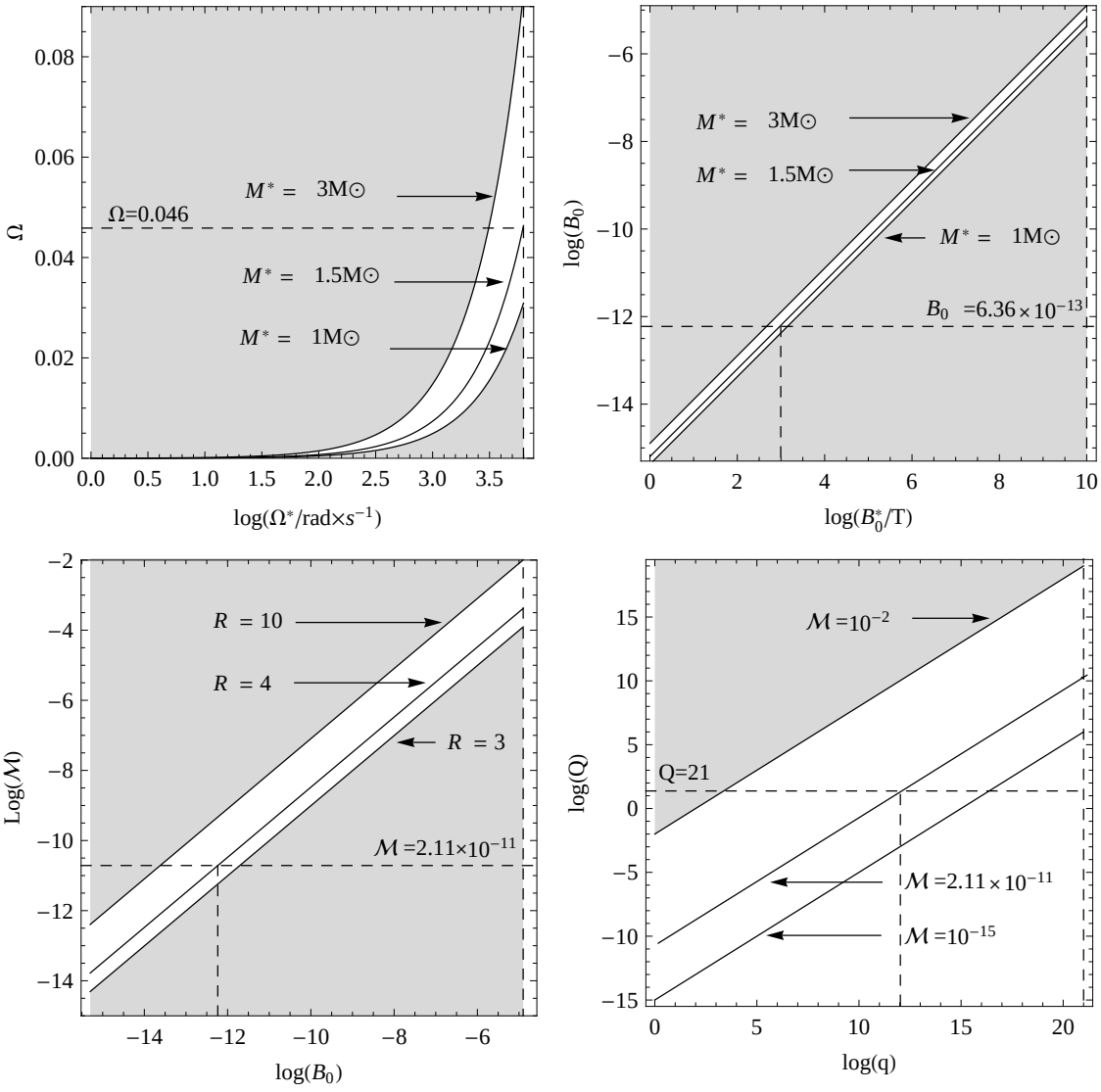

Figure 6. Relations between the physical parameters (magnetic field strength B_0^* and angular velocity of rotation Ω^*) and the corresponding scaled (dimensionless) parameters, characterizing a magnetic star and the charged particles moving around it. The dashed lines denote the assumed limits and some representative values. The gray regions are astrophysically irrelevant, within the assumed limitation.

For instance, a neutron star with the mass $M^* = 1.5\,\mathrm{M}_\odot$ (corresponding to the length-scale 2212 m), radius $R^* = 4M^* \doteq 8850\,\mathrm{m}$ and magnetic field strength $B_0^* = 10^3\,\mathrm{T} \doteq 2.87 \times 10^{-16}\,\mathrm{m}^{-1}$ ($\mathcal{M}^* \doteq 1.03 \times 10^{-4}\,\mathrm{m}^2$), rotating with the angular velocity $\Omega^* = 6283\,\mathrm{rad/s} \doteq 2.1 \times 10^{-5}\,\mathrm{m}^{-1}$ ($f^* \doteq 10^3\,\mathrm{Hz}$), is described by the scaled parameters $\Omega \doteq 0.046$ and $B_0 \doteq 6.36 \times 10^{-13}$ ($\mathcal{M} \doteq 2.11 \times 10^{-11}$). For particles with the specific charge $q = 10^{12}$ (charged dust grains), we have the effective specific charge $Q \doteq 21$ (see figure 6).

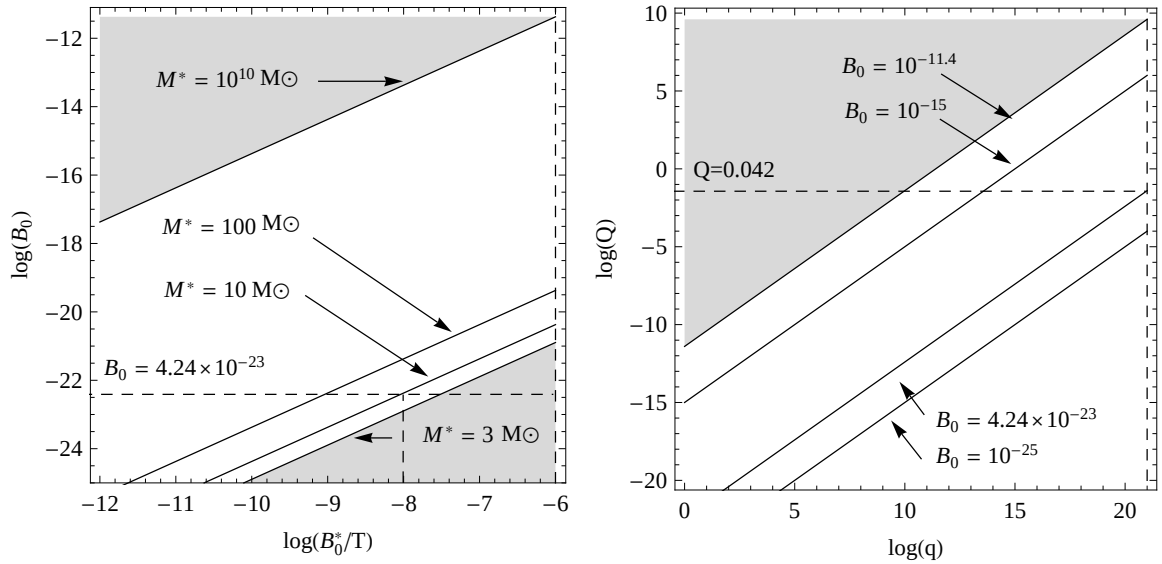

Figure 7. As in the previous figure, but for rotating black holes in the uniform magnetic fields.

5.2. Kerr black hole in uniform magnetic field

While masses of astrophysical black holes are known with relatively good precision and customarily categorized in three groups of stellar-mass black holes ($M^* \lesssim 30\,\mathrm{M}_\odot$), intermediate mass black holes ($10^2\,\mathrm{M}_\odot \lesssim M^* \lesssim 10^5\,M_\odot$), and supermassive black holes ($M^* \gtrsim 10^6\,\mathrm{M}_\odot$), much less is known about the intensity of cosmic magnetic fields surrounding the black holes. We assume masses of the black holes in the interval $3\,\mathrm{M}_\odot \leq M^* \leq 10^{10}\,\mathrm{M}_\odot$ [42,43] and the galactic magnetic field strength up to $B_0^* = 10^{-6}\,\mathrm{T}$. Near supermassive black holes with jets the magnetic field is thought to be still significantly stronger [44].

The limits of the used scaled parameters can be determined from the figure 7, which can be read in the following way. In the left plot, within the assumed astrophysically relevant values of the magnetic field strength $B_0^* \leq 10^{-6}$, we can determine values of B_0 for a fixed mass M^*. We can see that light black holes with $M^* = 3\,\mathrm{M}_\odot$ allow values of the scaled magnetic field strength up to $B_0 \doteq 10^{-20.9}$, while the heavy ones with $M^* = 10^{10}\,\mathrm{M}_\odot$ up to $B_0 \doteq 10^{-11.4}$. In the lower right plot, within the astrophysically relevant values of the specific charge $q \leq 10^{21}$, we can determine values of Q for a fixed scaled magnetic dipole strength B_0. We can see that weak magnetic field strengths of $B_0 = 10^{-25}$ allow values of the effective charge up to $Q = 10^{-4}$, while the strong ones of $B_0 = 10^{-11.4}$ up to $Q = 10^{9.6}$.

For instance, a rotating black hole with the mass $M^* = 10\,\mathrm{M}_\odot \doteq 14750\,\mathrm{m}$ in the asymptotically uniform magnetic field of the strength $B_0^* = 10^{-8}\,\mathrm{T} \doteq 2.87 \times 10^{-27}\mathrm{m}^{-1}$ is described by the parameter $B_0 \doteq 4.24 \times 10^{-23}$. For particles with the specific charge of magnitude $q = 10^{21}$ (electrons), we have the scaled effective charge $Q \doteq 0.042$ (see figure 7). Realistic values for the scaled spin a are limited by the value $a = 1$. For

the greater values of the spin, the black-hole horizons disappear and the Kerr metric describes the naked-singularity spacetime.

5.3. Possible applications

Two kinds of charged particles seem to be relevant with respect to the halo orbits. Firstly, in the case of electrons and protons, the magnitude of specific charges has a large value, and so the halo orbits can exist only very close to the black hole horizon or near an ultra-compact magnetic star. This kind of motion has been recently explored in the context of magnetospherical motion in stellar-mass black hole binaries [45]. Magnetically driven oscillations of matter near black holes have recently been explored also in the context of equatorial motion [33].

Another promising application of the halo motion concerns charged dust grains which typically acquire the magnitude of specific charge much smaller than that of elementary particles. Therefore, the gravitational effects influence the motion of dust grains more efficiently, and so they can form the halo orbits at larger distances from the star surface. Infrared observations are suitable to test the possible existence of halo orbits of dust grains around magnetic compact stars [25]. The debris discs of such particles could perturb the electromagnetic signal of the compact star and give rise to quasi-periodic modulation.

It is also well known that the frequencies of epicyclic geodesic motion [46, 47] have a substantial role in the resonant (or other) models of high-frequency quasiperiodic oscillation observed in the black hole [48–50] and neutron star [51] low mass X-ray binaries, and their magnetic-field induced modification could be of high importance, as shown in the case of equatorial motion [33].

6. Conclusions

Our calculations reveal the properties of halo motion of charged particles near magnetic compact stars and black holes. These can be relevant e.g. for charged dust grains when they acquire a small magnitude of electric charge and occur in the strong gravitational field. Such particles can originate from supernova material which falls back and migrates into the pulsar vicinity before evaporating.

The halo orbits can take place in axially symmetric systems: near a magnetic compact star, which we modelled by the Schwarzschild geometry and a test rotating dipole magnetic field, as well as near a Kerr black hole immersed in an asymptotically uniform magnetic field.

In this paper, we concentrated ourselves on the methodological aspects of the halo orbits and their systematic classification. Our main interest concerned the properties of the halo orbits in situations when the motion takes place in a strong gravitational field. We only briefly touched the astrophysical applications and will investigate them further in the following work. Table 3 summarizes the basic characteristics of different

examples of strongly gravitating systems which exhibit the halo orbits.

Table 3. Orientation of motion of electrically charged particles along stable halo orbits and the corresponding sign of the charge. The results correspond to the configuration where the magnetic field (characterized by the magnetic dipole moment $\mathcal{M}$ or magnetic field strength in the equatorial plane B_0) is oriented in the same direction as the rotation vector, characterized by the signs of Ω or a.

Compact object	Charge of particles	Orientation of motion
Rotating magnetic star	Positive	Co-rotation
	Positive	Counter-rotation
	Negative	Co-rotation
Static magnetic star	Positive	Counter-rotation
	Negative	Co-rotation
Magnetized black hole (Kerr metric)	Positive	Counter-rotation
	Negative	No-orbits

As for the magnetic compact stars, results of our discussion of the stable halo orbits orientation are qualitatively consistent with those obtained previously in Newtonian and the pseudo-Newtonian investigations [15, 18]. We notice that the strong gravitational field and the presence of event horizon affect the form of the effective potential and introduce significant changes with respect to the Newtonian case. However, we also notice that the pseudo-Newtonian approach can give surprisingly good information on the loci of halo orbits in spherically symmetric gravitational fields of magnetic stars, in which case the results qualitatively agree with the exact general relativistic approach presented here. On the other hand, the pseudo-Newtonian modelling of Kerr spacetimes [52, 53] is much more complicated, and seems to be less fruitful for modelling the phenomena in the Kerr geometry, which itself is relatively simple.

The effective potential of the halo motion exhibits a number of qualitatively different types. Two basic categories can be distinguished. The first one allows particles, bounded within the halo potential lobes, to commute across the equatorial plane. On the other hand, the second category does not allow such an interconnection, as the two lobes are entirely disjoint. The off-equatorial halo motion is an interesting phenomenon not only because it has not yet been explored in full detail in the literature, but also because it shows a variety of orbits, depending on orbital parameters: off-equatorial stable circular motion which does not cross the equatorial plane; small oscillations in the radial and vertical directions, with characteristic frequencies around the circular orbits; and the motion that traverses between the lobes when the energy is increased to sufficiently high levels. Recently, the off-equatorial motion of charged particles near Kerr black hole in asymptoticaly uniform magnetic field has been discussed from a different point of view in the ref. [54] as well.

Acknowledgments

The authors thank M. Urbanec for useful discussions concerning section 5.1. Institute of Physics and the Astronomical Institute have been operated under the projects MSM 4781305903 and AV 0Z10030501, and further supported by the Centre for Theoretical Astrophysics LC06014 in the Czech Republic. JK, VK and ZS thank the Czech Science Foundation (ref. P209/10/P190, 205/07/0052, 202/09/0772). OK acknowledges the doctoral student program of the Czech Science Foundation (ref. 205/09/H033).

References

[1] Chandrasekhar S 1983 *The Mathematical Theory of Black Holes* (Clarendon Press, Oxford)
[2] Misner C W, Thorne K S and Wheeler J A 1973 *Gravitation* (Freeman, San Francisco)
[3] Prasanna A R 1980 *Nuovo Cimento, Rivista* **3** 1
[4] Bičák J, Stuchlík Z and Balek V 1989 *Bulletin of the Astron. Inst. in Czechoslovakia* **40** 65
[5] Stuchlík Z, Bičák J and Balek V 1999 *General Relativity and Gravitation* **31** 53
[6] Prasanna A R and Sengupta S 1994 *Physics Letters A* **193** 25
[7] Vokrouhlický D and Karas V 1991 *Astronomy and Astrophysics* **243** 165
[8] de Felice F and Sorge F 2003 *Class. and Quantum Grav.* **20** 469
[9] Calvani M, de Felice F, Fabbri R and Turolla R 1982 *Nuovo Cimento B Serie* **67** 1
[10] Stuchlík Z and Hledík S 1998 *Acta Physica Slovaca* **48** 549
[11] Mestel L 1999 *Stellar Magnetism* (Clarendon Press, Oxford)
[12] Rezzolla L, Ahmedov B J and Miller J C 2001 *Mont. Not. Royal Astron. Soc.* **322** 723
[13] Petterson J A 1974 *Physical Review D* **10** 3166
[14] Wald R M 1974 *Physical Review D* **10** 1680
[15] Kovář J, Stuchlík Z and Karas V 2008 *Classical and Quantum Gravity* **25** 095011
[16] Stuchlík Z, Kovář J and Karas V 2009 *Proc. of the Int. Astr. Union, IAU Symposium* **259** 125
[17] Howard J E, Horányi M and Stewart G R 1999 *Physical Review Letters* **83** 3993
[18] Dullin H R, Horányi M and Howard J E 2002 *Physica D* **171** 178
[19] Stuchlík Z and Kovář J 2008 *Int. J. Mod. Phys. D* **17** 2089
[20] Paczyński B and Wiita P J 1980 *Astronomy and Astrophysics* **88** 23
[21] Abramowicz M A 2009 *Astronomy and Astrophysics* **500** 213
[22] Horanyi M 1996 *Annual Review of Astronomy and Astrophysics* **34** 383
[23] Cordes J M and Shannon R M 1998 *The Astrophysical Journal* **682** 1152
[24] Muno M P and Mauerhan J 2008 *The Astrophysical Journal* **648** L135
[25] Wang Zhongxiang, Chakrabarty D and Kaplan D L 2006 *Nature* **440** 772
[26] Duncan R C and Thompson C 1992 *The Astrophysical Journal* **392** L9
[27] Abramowicz M A, Nurowski P and Wex N 1995 *Classical and Quantum Gravity* **12** 1467
[28] Aguirregabiria J M, Chamorro A, Nayak K R, Suinaga J and Vishveshwara C V 1996 *Classical and Quantum Gravity* **13** 2179
[29] Stuchlík Z, Hledík S and Juráň J 2000 *Classical and Quantum Gravity* **17** 2691
[30] Kovář J and Stuchlík Z 2007 *Classical and Quantum Gravity* **24** 565
[31] Bardeen J M, Press W H and Teukolsky S A 1972 *The Astrophysical Journal* **178** 347
[32] Hartle J B, Thorne K S 1968 *The Astrophysical Journal* **153** 807
[33] Bakala P, Šrámková E, Stuchlík Z and Török G 2010 *Classical and Quantum Gravity* **27** 045001
[34] Lattimer J M and Prakash M 2004 *Science* **304** 536
[35] Lattimer J M and Prakash M 2007 *Physics Reports* **442** 109
[36] Bejger M, Haensel P and Zdunik J L 2007 *Astronomy and Astrophysics* **464** L49

[37] Haensel P, Zdunik J L, Bejger M and Lattimer J M 2009 *Astronomy and Astrophysics* **502** 605
[38] Glendenning N K 1997 *Compact stars. Nuclear physics, particle physics, and general relativity* Publisher: Berlin Springer
[39] Bahcall S, Lynn B W and Selipsky S B 1989 *Nuclear Physics B* **325** 606
[40] Miller J C, Shahbaz T and Nolan L A 1998 *Mont. Not. Royal Astron. Soc.* **294** L25
[41] Stuchlík Z, Török G, Hledík S and Urbanec M 2009 *Classical and Quantum Gravity* **26** 035003
[42] Ziolkowski J 2008 *Chines J. Astronom. Astrophys.* **8** (suppl.) 273
[43] Czerny B, Nikolajuk M 2009 *Frascati Workshop 2009, Multifrequency Behaviour of High Energy Cosmic Sources, Vulcano (Italy)* in press (arXiv:0910.0313)
[44] Reynolds C S, Garofalo D, Begelman M C 2006 *The Astrophysical Journal* **651** 1023
[45] Takahashi M and Koyama H 2009 *The Astrophysical Journal* **693** 472
[46] Aliev A and Galtsov D V 1981 *General Relativity and Gravitation* **13** 899
[47] Török G and Stuchlík Z 2005 *Astronomy and Astrophysics* **437** 775
[48] Török G, Abramowicz M A, Kluźniak W and Stuchlík Z 2005 *Astronomy and Astrophysics* **436** 1
[49] Stuchlík Z, Slaný P, Török G and Abramowicz M A 2005 *Physical Review D* **71** 024037
[50] Stuchlík Z, Slaný P and Török G 2007 *Astronomy and Astrophysics* **470** 401
[51] Török G, Bakala P, Stuchlík Z and Čech P 2008 *Acta Astronomica* **58** 1
[52] Semerák O and Karas V 1999 *Astronomy and Astrophysics* **343** 325
[53] Mukhopadhyay B 2002 *The Astrophysical Journal* **581** 427
[54] Preti G 2010 *Physical Review D* **81** 024008